Journal of Cerebral Blood Flow & Metabolism (2011) 31, 1986–1998

www.jcbfm.com

Review Article

Image-derived input function for brain PET studies: many challenges and few opportunities

Paolo Zanotti-Fregonara[1], Kewei Chen[2,3], Jeih-San Liow[1], Masahiro Fujita[1] and Robert B Innis[1]

[1]*Molecular Imaging Branch, NIMH, NIH, Bethesda, Maryland, USA;* [2]*Banner Alzheimer's Institute and Banner Good Samaritan PET Center, Phoenix, Arizona, USA;* [3]*Department of Mathematics and Statistics, Arizona State University, Tempe, Arizona, USA*

Quantitative positron emission tomography (PET) brain studies often require that the input function be measured, typically via arterial cannulation. Image-derived input function (IDIF) is an elegant and attractive noninvasive alternative to arterial sampling. However, IDIF is also a very challenging technique associated with several problems that must be overcome before it can be successfully implemented in clinical practice. As a result, IDIF is rarely used as a tool to reduce invasiveness in patients. The aim of the present review was to identify the methodological problems that hinder widespread use of IDIF in PET brain studies. We conclude that IDIF can be successfully implemented only with a minority of PET tracers. Even in those cases, it only rarely translates into a less-invasive procedure for the patient. Finally, we discuss some possible alternative methods for obtaining less-invasive input function.
Journal of Cerebral Blood Flow & Metabolism (2011) **31,** 1986–1998; doi:10.1038/jcbfm.2011.107; published online 3 August 2011

Keywords: image-derived input function; kinetic modeling; neuroreceptor tracers; PET

Introduction

Quantitative positron emission tomography (PET) brain studies often require that input function be measured. This is traditionally performed via the invasive procedure of arterial cannulation. Arterial cannulation is not that dangerous (Everett *et al*, 2009). For instance, >3000 PET-related arterial cannulations have been performed at the National Institutes of Health; only two cases of minor local complications occurred, and both were readily resolved by the attending physician. Arterial cannulation is, however, a laborious procedure for the research personnel and often discourages patients and healthy volunteers from participating in clinical research.

Image-derived input function (IDIF) appears to be an elegant and attractive noninvasive alternative to arterial sampling that obviates the need for arterial cannulation, blood handling and analysis, and additional radiation exposure of the research personnel. Image-derived input function has been successfully validated using large blood pools, such as the heart (Choi *et al*, 1991), the aortic segments (van der Weerdt *et al*, 2001), and the femoral arteries (Ludemann *et al*, 2006). Given the large size of these vascular structures, partial volume effects can be easily corrected or even neglected (van der Weerdt *et al*, 2001). However, because in brain PET studies these large blood pools are not in the field of view, IDIF must rely on intracranial blood vessels. Carotid arteries, the most often used intracranial blood vessels, have an average diameter of about 5 mm (Krejza *et al*, 2006), and the spatial resolution of modern PET cameras is about 6 mm (Brix *et al*, 1997). This limited spatial resolution entails two highly linked partial volume effect artifacts: (1) a 'spill-out' effect (i.e., the activity contained within

Correspondence: Dr RB Innis, Molecular Imaging Branch, National Institute of Mental Health, Building 10, Room B1D43, 31 Center Drive, MSC-1026, Bethesda, MD 20892-2035, USA.
E-mail: innisr@mail.nih.gov
This study was supported by the Intramural Research Program of the National Institute of Mental Health, National Institutes of Health, Department of Health and Human Services (IRP-NIMH-NIH-DHHS), by the National Institute of Mental Health, US (RO1 MH57899), the National Institute on Aging, US (R01AG031581-10 and P30 AG19610), and the state of Arizona.
Received 1 April 2011; revised 24 May 2011; accepted 29 June 2011; published online 3 August 2011

the carotid spreads over the surrounding tissue, so that the measured activity is lower than the actual activity) and (2) a 'spill-in' effect (i.e., the activity from surrounding tissues spills into the carotid, so that the measured activity is artificially increased). These two artifacts alter both the amplitude and the shape of the carotid signal. The former is responsible for an underestimation of the input function; the latter accounts for an artificial elevation of carotid activity and potentially changes the curve shape. To obtain a good estimate of the input function, both these effects should be corrected.

Using the carotid arteries as an example, computation of IDIF for brain PET studies requires three steps: (1) carotid identification, which can be achieved by using coregistered anatomic images or segmenting the carotids directly on the PET images; (2) the whole-blood time–activity curve estimation, which is achieved by correcting partial volume effects; and (3) the concentration of parent radioligand in plasma, separated from radiometabolites, must be estimated as a percentage of the previously determined concentration of total radioactivity in blood. This third step requires either a prior knowledge or *in vitro* analysis of blood samples, because the PET image cannot distinguish the chemical structures (e.g., parent versus radiometabolite) from which the photons are emitted. Solving these three steps is a challenging task. As a result, IDIF is still very rarely used in clinical practice despite the increased number of PET brain imaging studies conducted in recent years.

The aim of the present review was to identify the methodological challenges that hinder the widespread use of IDIF in PET brain studies. We conclude that IDIF can be successfully used only in selected situations. From the patient's perspective, it allows for less-invasive estimates of input function only for a minority of tracers. Finally, we discuss some other alternative methods for obtaining the input function in a less-invasive manner than serial blood sampling.

How Often is Image-derived Input Function Used in Positron Emission Tomography Brain Studies?

Over the last 15 years, a large number of studies aimed at validating IDIF methods using brain vessels have been published (Ahn *et al*, 2000; Asselin *et al*, 2004; Backes *et al*, 2009; Baudrexel *et al*, 2004; Bentourkia, 2005; Berradja *et al*, 2009; Bodvarsson *et al*, 2006; Carson *et al*, 2006; Chen *et al*, 1998, 2007, 1996; Croteau *et al*, 2010; Fadaili el *et al*, 2009; Fung *et al*, 2009; Guo *et al*, 2007; Kim *et al*, 2001; Liptrot *et al*, 2004; Litton, 1997; Maroy *et al*, 2011; Mourik *et al*, 2008*a*, *b*, 2009; Naganawa *et al*, 2005*a*, *b*; Nishizawa *et al*, 1998; Parker and Feng, 2005; Sanabria-Bohorquez *et al*, 2003; Sayre and Seo, 2009; Su *et al*, 2005; Trebossen *et al*, 1999; Verhaeghe *et al*, 2010; Wahl *et al*, 1999; Wang *et al*, 2009; Zanotti-Fregonara *et al*, 2007). These methods incorporated a variety of imaginative, and often clever, approaches. Nevertheless, these investigations did not prompt widespread adoption of IDIF and, indeed, the number of clinical research protocols using IDIF as a tool to reduce invasiveness in patients is very limited. Chen *et al* used their IDIF method for [^{18}F]-FDG (Chen *et al*, 1998) to measure cerebral metabolic rate for glucose in young adults at genetic risk for late-onset Alzheimer's dementia (Reiman *et al*, 2004), to differentiate healthy subjects from Alzheimer's patients (Chen *et al*, 2006), and to evaluate healthy adults reporting dream-enactment behaviors (Caselli *et al*, 2006). Schiepers *et al* used an IDIF method based on factor analysis to study patients with brain tumors using [^{18}F]-fluorothymidine (Schiepers *et al*, 2007*b*) and [^{18}F]-FDOPA (Fueger *et al*, 2010; Schiepers *et al*, 2007*a*). Although this method was never validated for brain studies against a reference input function, especially vis-à-vis the recovery coefficient used for partial volume correction, Schiepers *et al* had previously shown that it yielded reliable input functions for bone disorders with [^{18}F]-fluoride (Schiepers *et al*, 1997), in breast cancer with [^{18}F]-FDG (Schiepers *et al*, 1998), in prostate cancer with [^{11}C]-acetate (Schiepers *et al*, 2000, 2002*b*, 2008) and in myocardial studies with [^{13}N]-ammonia, [^{15}O]-H_2O, and [^{18}F]-FDG (Schiepers *et al*, 2002*a*; Wu *et al*, 1995).

In addition, several other examples of clinical research protocols using IDIF exist (Beer *et al*, 2007; Wang *et al*, 2010). In these studies, IDIF was simply the raw carotid time–activity curve obtained by placing ROIs (regions-of-interest) over the carotid arteries, without any correction for partial volume effect artifacts. Comparing to the total distribution volume (V_T) obtained with arterial sampling in [^{11}C]-PIB PET study, Lopresti *et al* (2005) found an overestimation of V_T by a factor of two with the use of the raw carotid time–activity curves without correction for partial volume effect.

Thus, despite a huge number of published studies exploring different IDIF methods and the obvious interest in avoiding arterial blood sampling, IDIF was actually used as a tool to reduce invasiveness only in very few PET procedures.

How Should Carotids be Segmented?

With the exception of algorithms that work without any prior anatomical assumption, such as blind source separation algorithms when they are used to derive directly the input function through the source signal mixing process (Bodvarsson *et al*, 2006; Naganawa *et al*, 2005*a*), the initial step in calculating IDIF is carotid segmentation, which is required for obtaining raw blood time–activity curves. Carotid segmentation has been performed by both taking

advantage of coregistered magnetic resonance images (MRI) (Fung *et al*, 2009; Litton, 1997; Trebossen *et al*, 1999), and by placing carotid ROIs directly on PET images (Chen *et al*, 1998; Liptrot *et al*, 2004; Mourik *et al*, 2008*a*; Su *et al*, 2005).

In theory, MRI segmentation should be the reference method since it would allow a better identification of the overall carotid diameter over the entire length of the vessel. However, in practice, reliable MRI-based PET carotid segmentation is very difficult to achieve. Existing coregistration algorithms are based on brain structures above the location of the carotids. Therefore, an overall good brain coregistration can still potentially lead to inaccurate coregistrations of the carotid arteries (Fung *et al*, 2009). Moreover, the carotid is a small, elongated, and elastic object, which can be stretched, bent, and twisted depending on the position of the head relative to the rest of the body. As a result, a difference in head positioning between PET and MRI could engender alignment errors that cannot be corrected by simple rigid-body coregistration. Mourik *et al* (2008*a*) showed that use of MRI images coregistered to [^{11}C]-flumazenil images often resulted in erroneous definition of the carotid arteries, which in turn led to IDIF estimation errors. Fung *et al* (2009) studied an MRI-based approach to segment carotids for PET and found that it was often necessary to independently coregister the left and right carotids using complex coregistration algorithms, given that the degree of carotid mismatch between the PET and MRI images within the same subject could be more pronounced for one carotid than for the contralateral one. The introduction of hybrid PET/MRI devices may eliminate this problem. Nevertheless, for the time being, carotid segmentation performed directly on PET images seems to be a better option, because it obviates the need to acquire an MRI and is not affected by coregistration errors described above. It is certainly true that segmentation on PET images may prove difficult due to the low signal-to-noise ratio in short-duration PET images (Fung *et al*, 2009). However, in our experience, carotid arteries are almost always easily recognizable on the early summed frames of a dynamic PET scan after a bolus injection of the tracer. Moreover, it can also be argued that if a tracer gives a carotid signal that is too weak and noisy to be clearly distinguishable by the human eye, such a signal would hardly be amenable to reliable quantification.

Positron emission tomography carotid artery segmentation techniques, some of which are based on the selection of a limited number of hot voxels inside the carotid (Croteau *et al*, 2010; Mourik *et al*, 2008*a*), can be either manual (Chen *et al*, 1998), or automatic working directly on dynamic PET data. Examples of these automatic algorithms are *k*-means clustering (Liptrot *et al*, 2004), independent component analysis, when used to determine the spatial coordinates of the carotids (Chen *et al*, 2007; Su *et al*, 2005), an algorithm based on analysis of local minima (Zanotti-Fregonara *et al*, 2009*b*) or a graph-based Mumford-Shah energy-minimization algorithm (Parker and Feng, 2005). Automatic algorithms may save time and reduce interoperator and intraoperator variability, but it is not clear whether they may provide more accurate kinetic modeling results (Chen *et al*, 1998, 2007). (Throughout the manuscript, the word 'accurate' is used to indicate a measure that is both precise and unbiased.)

Although segmentation of PET images avoids problems associated with the multimodality coregistration, estimating carotid anatomical parameters such as its volume would be less accurate. An accurate estimate of carotid volume is necessary if partial volume effect correction is to be performed by applying recovery coefficients calculated from the anatomy of the vessel. Below, we argue that precise estimates of the geometry and diameter of the carotids should not be an essential requirement for calculating IDIF. In fact, estimates conducted using recovery coefficients are prone to errors and scaling with one or more blood samples should be preferred.

Can Blood Sampling Really be Avoided?

An ideal IDIF method would completely eliminate the need for blood sampling. Although some methods do require at least one blood sample to scale the image input (Berradja *et al*, 2009; Chen *et al*, 1998; Guo *et al*, 2007; Naganawa *et al*, 2005*a*; Sanabria-Bohorquez *et al*, 2003), most recently published methods are completely blood free (Backes *et al*, 2009; Carson *et al*, 2006; Croteau *et al*, 2010; Mourik *et al*, 2008*a*).

One of the most commonly used and simplest approaches for noninvasive scaling is the use of empirically determined recovery coefficients, which are calculated when the volume of the vessel and the scanner characteristics are known (Carson *et al*, 2006; Croteau *et al*, 2010; Litton, 1997). Despite being simple to implement, this approach may not be very robust for the following reasons: (1) given the very small size of the carotids, even small inaccuracies in estimating carotid volume would create significant errors in estimating the recovery coefficient; (2) recovery coefficients are usually obtained from spherical or cylindrical phantoms (hence the carotid volume estimation being simplified to its diameter), which may not simulate the shape of the carotids very well; and (3) the uncorrected carotid time–activity curve is never a scaled-down curve with the same shape of the measured arterial input function. Lopresti *et al* (2005) compared [^{11}C]-PIB carotid time–activity curves that were not corrected for partial volume effect to the measured arterial input function, and found that the two sets of curves had a very different shape. At the beginning of the scan (<5 minutes), the carotid input function underestimated the arterial input function by as much as a

factor of four, while at later times (>5 minutes), mainly because of spill-in, the two curves tended to converge and the ratio was at about 2. These findings are consistent with our own experience.

Croteau *et al* (2010) derived recovery coefficients by measuring carotid diameter on the computed tomography scan of each subject. Although the results of kinetic modeling performed with the corrected IDIF were good, the method appeared to be very sensitive to errors of carotid diameter estimation. Underestimating the diameter of the carotid artery by just 1 mm would entail an error in the cerebral metabolic rate of [^{18}F]-FDG of about 17%. Even larger errors were found when this method was applied to femoral arteries using [^{11}C]-acetate; an under/overestimation of the artery size of 1 mm induced an under/overestimation of about 66% in the perfusion index (Croteau *et al*, 2010).

In the study by Carson *et al* (2006), individual recovery coefficients were obtained from MR images of carotids and then used to correct high-resolution research tomograph (HRRT) [^{15}O]-H_2O PET scans. Compared with the reference arterial input function, IDIF had a substantially higher peak (+29%). Furthermore, errors of 15% to 19% were found in the flow images obtained using autoradiographic quantification method with IDIF compared with the values with arterial sampling.

Using a camera with a larger axial field of view will have the carotid arteries positioned further away from the edge of the field-of-view and may allow imaging the carotids further down the neck, where the carotid diameter is larger and hence the quantification more reliable.

This inaccuracy due to the use of recovery coefficients can be reduced, but not eliminated, by using intracranial venous sinuses, which have a larger volume than carotid arteries (Asselin *et al*, 2004; Nishizawa *et al*, 1998; Schiepers *et al*, 2007*b*; Wahl *et al*, 1999). Schiepers *et al* (2007*b*) used a fixed recovery coefficient to scale factor analysis based input functions from transverse sinuses. However, the accuracy of this scaling was not tested against the gold standard of arterial input function. Nishizawa *et al* (1998) tried to obtain an IDIF from the confluence of venous sinuses for α-[^{11}C]-methyl-tryptophan PET scans but could not find a fixed recovery and spillover coefficient; individual sinus curves thus had to be normalized using venous samples. A study by Asselin *et al* (2004) nicely describes the challenges and possible sources of error associated with noninvasive recovery of radioactivity concentration from the sagittal venous sinuses. The investigators noted that an accurate estimate of radioactivity concentration could be obtained only in a phantom composed of radioactive cylinders if the point spread function was accurately determined at the location of the cylinders, after careful selection of the smoothing filters. When the method was tested in humans, the results were less reliable (Asselin *et al*, 2004).

Moreover, the venous sinus provides the concentration of tracer in the vein, whereas we seek its concentration in the artery as the input function.

Some methods select a limited number of hot voxels (such as the voxel with maximal intensity) from inside the carotid, which are assumed to be free of partial volume effects (Mourik *et al*, 2008*a*; Parker and Feng, 2005; Su *et al*, 2005). These methods are attractive because they are very easy to implement, and because they do not rely on precise estimates of vessel diameter to calculate a recovery coefficient. However, it should be noted that these methods are validated *a posteriori* on a given set of scans by fine-tuning many imaging parameters including the choice of reconstruction algorithm, scatter correction method, filters, and the setting associated with each of them. Moreover, the accuracy is also heavily and unpredictably influenced by the measurement noise and tracer biodistribution. For example, Mourik *et al* (2008*a*, *b*) demonstrated that their method allowed the calculation of a blood-free IDIF when applied to [^{11}C]-flumazenil using a standard PET camera, but not when [^{11}C]-flumazenil scans were acquired using a HRRT. Because the resolution of HRRT is higher (~2.5 mm) than that of a standard PET camera (~6 mm), the less accurate results obtained by Mourik with a HRRT may have been caused by the presence of additional sources of errors that offset the advantages of the camera's higher spatial resolution. In this case, the sources of errors were likely the higher scatter fraction and higher noise levels associated with HRRT images. Additional investigations found that this method allowed a blood-free IDIF when applied to *(R)*-[^{11}C]verapamil scans, but not when applied to [^{11}C]-PIB, *(R)*-[^{11}C]-PK11195 (Mourik *et al*, 2009) or [^{18}F]-FDG (Zanotti-Fregonara *et al*, 2009*a*). Parker and Feng (2005) showed that their blood-free method worked well when [^{18}F]-FDG scans were reconstructed with an iterative expectation-maximization algorithm, but not when the same scans were reconstructed with filtered backprojection.

In summary, the extant evidence suggests that, given the small size of intracranial blood vessels, a robust partial volume effects correction is very difficult to achieve using only image processing approaches, even with high-resolution images (Zanotti-Fregonara *et al*, 2011*a*). In our opinion, scaling with blood samples is the most reliable option. Moreover, because uncorrected curves do not have the same shape as the measured arterial input function, it is also likely that more accurate results would be obtained by scaling with more than one blood sample together with the correction of the spill-in contamination from the surrounding tissue (Chen *et al*, 1998).

Three comparative studies, where different IDIF methods were directly compared on the same scans, suggest that IDIF methods that rely on blood samples provide a more accurate estimate of input function than blood-free methods (Chen *et al*, 2007;

Zanotti-Fregonara *et al*, 2009*a*, 2011*a*). As explained in the following section, blood samples (and probably more than one) are also necessary for obtaining the concentration of unchanged parent in plasma.

The Issue of Metabolite and/or Plasma Versus Whole-blood Correction

With some notable exceptions such as [^{18}F]-FDG, almost all tracers used in brain imaging produce variable amounts of radiometabolites. One important limitation of IDIF is that it cannot distinguish the parent compound from its radioactive metabolites and the plasma radioactivity to that of whole blood. Some IDIF methods for neuroreceptor tracers described in the literature estimated only the whole-blood curve from images, and the percentage of unchanged parent was obtained at each time point by correcting the image input using HPLC (high-performance liquid chromatography) analysis from arterial blood sampling (Mourik *et al*, 2008*a*, 2009), thus diminishing the practical utility of the method. In some other studies, the problem of individual metabolite correction was not taken into account (Litton, 1997; Naganawa *et al*, 2005*b*). Naganawa *et al* (2005*b*) calculated [^{11}C]-MPDX whole-blood time–activity curve using independent component analysis and suggested that these curves could be used for absolute V_T quantification, because the metabolite fraction for this tracer was negligible. However, a previous study found that 76% of administered [^{11}C]-MPDX remained intact 60 minutes after injection (Kimura *et al*, 2004). The question remains whether an error of up to $\sim$25% in parent concentration levels can be safely overlooked. Indeed, [^{18}F]-FLT has a biokinetic behavior that is very similar to that of [^{11}C]-MPDX, with a mean amount of unaltered [^{18}F]-FLT of 74% at 60 minutes (Shields *et al*, 2005). If all blood activity is assumed to be unaltered [^{18}F]-FLT, kinetic modeling would yield a mean error of 19.6% in the estimated compartmental flux, with a range of 14.9% to 30.2% (Shields *et al*, 2005).

Individual metabolite correction can occasionally be successfully integrated in the IDIF procedure, but some blood samples are necessary; thus, the only advantage of IDIF over arterial input function would be a reduced number of arterial blood samples. Using [^{11}C]-flumazenil scans, Sanabria-Bohorquez *et al* (2003) showed that an IDIF calculated from carotid arteries could be used to reduce the number of necessary blood samples to five or six. These blood samples were used both to estimate the parent fraction in plasma and to scale the IDIF. A previous study with [^{11}C](*R*)-rolipram from our laboratory demonstrated that a reliable metabolite-corrected input function could be achieved using a carotid IDIF and only four arterial blood samples (Zanotti-Fregonara *et al*, 2011*b*). The blood samples were used to calculate the recovery and the spill-in coefficients by linear least-squares analysis and also to obtain the parent concentration by fitting a monoexponential function through the parent/whole-blood ratio calculated by HPLC analysis in those same four blood samples. It must be noted that to successfully estimate the metabolite curve with a limited number of blood samples, the metabolite curve should be amenable to simple modeling. For [^{11}C](*R*)-rolipram, we were able to reliably calculate the parent fraction with only four blood samples because the parent/whole-blood ratio over time was well fitted to a monoexponential function. Had this curve been more complex, more blood samples would have been required and the practical utility of the IDIF method would have been questionable.

One practical way to estimate the radiometabolites concentrations without arterial sampling would be to use some late venous blood samples, when the metabolite concentration is maximal and arteriovenous equilibrium has been reached. This approach must, however, be validated for each tracer, but it is not always feasible. For instance, even when the whole-blood concentration of [^{11}C](*R*)-rolipram is the same between the arterial and venous blood (30 to 40 minutes after injection), the relative concentrations of parent and radiometabolites are still different and, therefore, venous samples cannot be used to estimate the arterial radiometabolite concentrations (our unpublished data).

To completely avoid blood sampling, an average metabolite curve may be used. This type of metabolite correction is not always possible and must be validated for each tracer. An average metabolite curve may work well for some tracers, such as [^{11}C]-raclopride (Lammertsma *et al*, 1996), 2[^{18}F]F-A-85380 (Mitkovski *et al*, 2005), or [^{18}F]-FLT (Backes *et al*, 2009). Occasional outliers should nevertheless be expected when using an average metabolite correction and its applicability in research protocols must be carefully evaluated. For [^{18}F]-FLT, the difference in parent concentration between the population mean and the range values is often about 15% to 20% toward the end of the scan (Shields *et al*, 2005; Visvikis *et al*, 2004). Moreover, the average value obtained from a given population may not be transferable to a different population. For instance, [^{18}F]-FLT is metabolized in the liver via glucuronidation (Visvikis *et al*, 2004), and any disease or therapeutic agent that affects hepatic function is likely to affect the input function to the brain by changing the amount of radiometabolites. Finally, the amount of metabolites may also differ among healthy subjects due to physiologic characteristics (e.g., gender) (Beierle *et al*, 1999; Henriksen *et al*, 2006).

The published literature and our personal experience suggest that an average metabolite curve cannot be used for most tracers. With the aim of avoiding individual metabolite correction, Ishiwata *et al* (1998) analyzed [^{11}C]-flumazenil radiometabolites in 24 subjects. They found that when the mean

fraction of unchanged [^{11}C]-flumazenil at each time point was used instead of individually measured metabolite data for the arterial input function, an error of as much as 30% occurred in the [^{11}C]-flumazenil V_T. Sanabria-Bohorquez *et al* (2000) devised a method to determine the parent fraction of [^{11}C]-flumazenil in plasma using the information contained in the tissue kinetic PET data and a three-injection protocol, though blood sampling was still required to estimate total radioactivity in plasma. Our laboratory obtained very reliable results in 12 subjects whose whole-blood [^{11}C](*R*)-rolipram IDIFs were corrected for radiometabolites at each time point using the gold standard of individual HPLC analyses. The image/blood Logan-V_T ratio was 0.99 ± 0.04 and all the subjects had a V_T estimation error of $<10\%$ (range 0.93 to 1.05). However, when the same IDIF curves were corrected using an average metabolite curve calculated from these same 12 subjects, a much greater standard deviation was obtained (image/blood Logan-V_T ratio of 0.98 ± 0.20), and only three of the 12 subjects had a V_T estimation error $<10\%$ (range 0.76 to 1.44) (Zanotti-Fregonara *et al*, 2011*a*).

In addition to metabolites, the implicit assumption when using IDIF is that the difference between the plasma tracer concentration and the one in whole blood is negligible. This assumption may be true for [^{18}F]-FDG (Gambhir *et al*, 1989) or [^{18}F]-FLT (Visvikis *et al*, 2004), but not for many other tracers. For instance, blood cells have binding sites for some tracers such as those for the translocator protein (Kreisl *et al*, 2010) and for serotonin transporters (Ichise *et al*, 2003). Specific binding to cells can cause uneven distribution between cells and plasma, and some blood samples are therefore necessary to determine plasma concentration. Even in the case of [^{18}F]-FDG, some blood samples must be taken to measure blood glucose levels, which are required for quantifying the cerebral metabolic rate of glucose (Wienhard, 2002).

Why Does a Method Work for One Tracer but not Another?

Methods that are validated and work well with a given tracer may not perform equally well when applied to a different one (Mourik *et al*, 2009; Zanotti-Fregonara *et al*, 2011*a*). For instance, using the IDIF method validated by Chen *et al* (1998) for [^{18}F]-FDG, our laboratory obtained excellent results with [^{11}C](*R*)-rolipram scans (Zanotti-Fregonara *et al*, 2011*b*), but equally accurate results could not be obtained with any other tracer of our database. Indeed, IDIF methods seem to be very tracer specific. At least two factors have a major role in the accuracy of IDIF: tracer kinetics, which affects the accuracy of the image-derived whole-blood estimate, and the amount of radiometabolites, which affect the final results of kinetic modeling.

In our experience, a good estimate of the whole-blood curve cannot be obtained for most tracers. Depending on their kinetics after a bolus injection, tracers may show a strong or weak carotid signal as well as uptake in the surrounding tissues (Figures 1A–1D). The whole-blood curve can be estimated well only if the tracer gives an adequate carotid to background ratio, and this is not the case for many tracers—including [^{18}F]-FMPEP-d_2, [^{11}C]-MePPEP, [^{11}C]-DASB, and [^{18}F]-SP203—where a high early uptake in the surrounding tissues blurs the carotid signal. Even for those tracers where good estimates of the whole-blood curve can be achieved, the accuracy of kinetic modeling results may be influenced by the amount of radiometabolites. The importance of radiometabolites is underscored by this example of two radioligands: [^{11}C](*R*)-rolipram, a tracer for brain phosphodiesterase 4, and [^{11}C]-PBR28, a tracer for the translocator protein. These tracers have a very different metabolite profile: [^{11}C](*R*)-rolipram produces few metabolites and, 90 minutes after injection, the parent/whole blood ratio is about 80%. In contrast, [^{11}C]-PBR28 is quickly metabolized and, 90 minutes after injection, parent/whole blood ratio is only about 7% (Zanotti-Fregonara *et al*, 2011*a*). Some IDIF methods allowed us to obtain a good estimate of the whole-blood curves for both tracers, with mean ratios between the image and whole-blood area under the curve close to one. Regardless of the IDIF method used, however, after metabolite correction and kinetic modeling, V_T estimates were always more accurate for [^{11}C](*R*)-rolipram than for [^{11}C]-PBR28 (Zanotti-Fregonara *et al*, 2011*a*). The reason is easy to understand. Because of coarse PET framing, even a good-quality IDIF would typically show inaccuracies in peak estimation, while tails were generally well estimated. This is usually not important, because graphical methods (Patlak, Logan) rely on the area under the curve, and the peak contributes very little to the total area under the curve. [^{11}C](*R*)-rolipram is slowly metabolized and remains the predominant portion of blood radioactivity throughout the scan. Therefore, even after metabolite correction, the area under the peak is always negligible as compared with the total area under the entire curve (Figures 2A and 2B). In contrast, for [^{11}C]-PBR28, the tail comprises mostly radiometabolites. Therefore, even if the whole-blood curve is well estimated, after metabolite correction, the area under the tail dramatically decreases and the unreliable peak now accounts for a larger proportion of the total area under the curve (Figures 2C and 2D). Unfortunately, most neuroreceptor tracers have a high metabolite fraction and would therefore not be easily amenable to IDIF quantification.

It is not easy to directly measure the input function peaks using PET cameras. Even with a list-mode acquisition, the frame durations cannot be too short, or the noise would prevent a reliable quantification. In addition to the physical limitations intrinsic to the machine, it is also difficult to find a single analytical

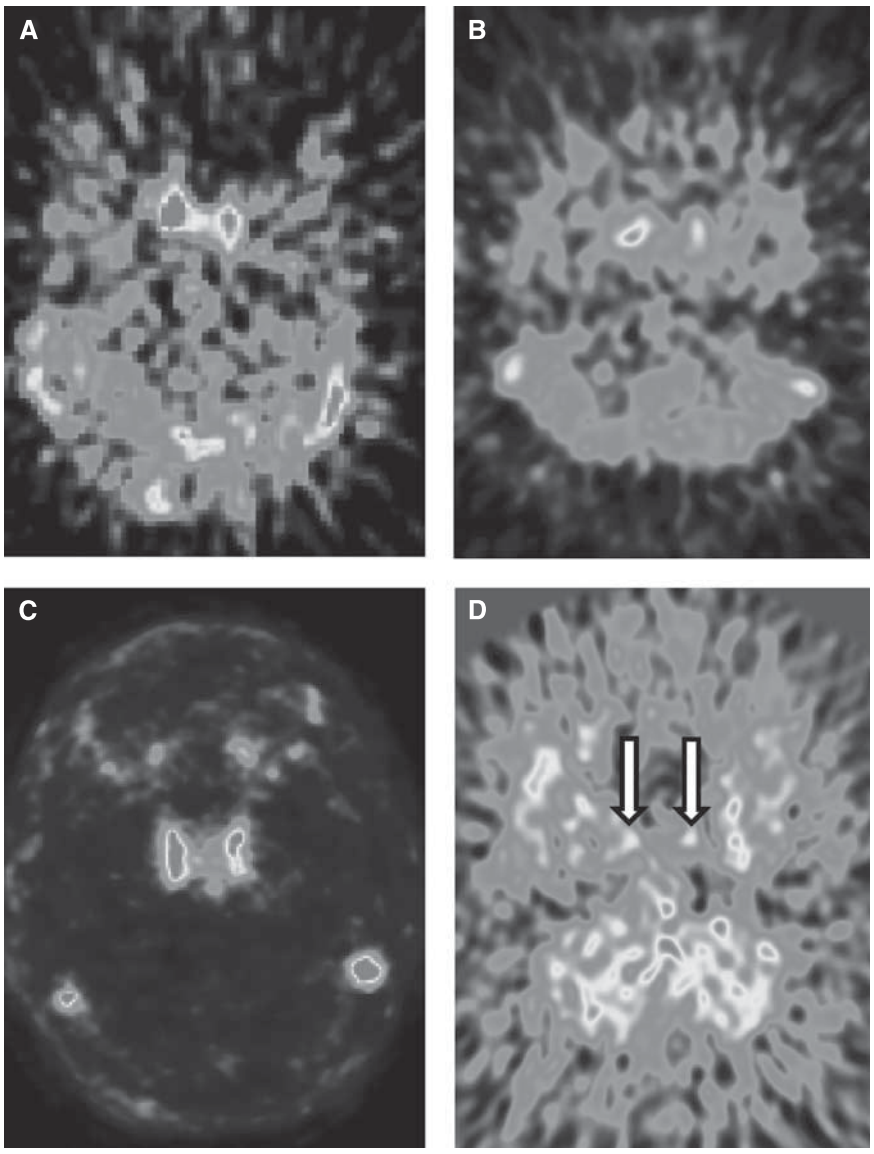

Figure 1 Early summed frames of [^{11}C](*R*)-rolipram, [^{18}F]-FMPEP-d_2, [^{11}C]-*N*-desmethyl-loperamide, and [^{11}C]-DASB. These four tracers show different biodistributions and carotid/background ratio. [^{11}C](*R*)-rolipram (**A**) shows a strong carotid signal, with a relatively low spill-in from the background tissues. Whole-blood time–activity curves could thus be reliably estimated from the images (Zanotti-Fregonara *et al*, 2011*b*). In contrast, [^{18}F]-FMPEP-d_2 (**B**) shows a higher spill-in from surrounding regions, probably due to its higher lipophilicity. This spill-in could not be well corrected, and the whole-blood time–activity curves generally showed a low peak and a progressively increasing tail. [^{11}C]-*N*-desmethyl-loperamide (**C**) is a substrate for the P-gp efflux protein at the blood–brain barrier. Therefore, the carotid/background ratio is excellent, because there is virtually no background activity. Nevertheless, reliable whole-blood time–activity curves could not be obtained, probably because the images were too noisy and iterative reconstruction algorithms may not quantify 'cold zones' well (the raw carotid time–activity curves often showed a much higher concentration of activity than the corresponding arterial blood samples). Finally, in [^{11}C]-DASB scans (**D**), the carotids (indicated with arrows) are curiously almost invisible. Although carotids could be delineated using a coregistered magnetic resonance image (MRI), the signal is too faint to be reliably quantified. The color reproduction of this figure is available at the HTML version of this article.

formulation capable of yielding a good model of tracer concentration for both the peak and the tail (Guo *et al*, 2007). To address this problem, Guo *et al* (2007) estimated the peak and tail of [^{18}F]-FDG input function using two different approaches. The peak was modeled as a triangle whose three nodes were obtained from image-derived data from carotid arteries; the tail was estimated using a simultaneous estimation (SIME) approach associated with three blood samples. Sanabria-Bohorquez *et al* (2003) used a blood-calibrated IDIF to estimate the tail of [^{11}C]-flumazenil input functions, while the peak was recovered by adding an exponential function to the scaled curve whose parameters were estimated

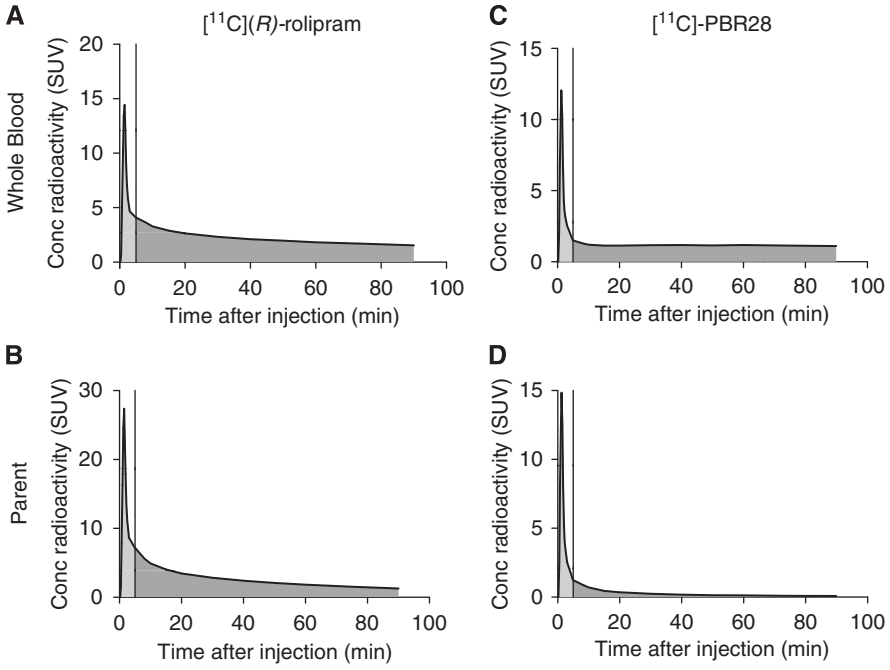

Figure 2 Representative blood time–activity curves obtained from arterial sampling for [^{11}C](*R*)-rolipram (left column) and [^{11}C]-PBR28 (right column). The area under the curve of the peak (shaded in blue) is usually difficult to estimate reliably because it is characterized by rapid changes of radioactivity over time, while the area under the curve of the remaining part (the tail, shaded in green) is easier to estimate. [^{11}C](*R*)-rolipram whole-blood time–activity curves (**A**) are generally well estimated. In addition, [^{11}C](*R*)-rolipram is slowly metabolized and even after metabolite correction, the area under the peak is always negligible compared with the total area under the curve (**B**). [^{11}C]-PBR28 whole-blood time–activity curves (**C**) are also well estimated. However, because the tail comprises mostly radiometabolites, after metabolite correction the area under the tail dramatically decreases and the unreliable peak now accounts for a larger proportion of the total area under the curve (**D**). Please note that the SUV concentration of the parent can be higher than that of the whole-blood, because the parent values refer to the concentration in the plasma. The color reproduction of this figure is available at the HTML version of this article.

from brain time–activity curves using SIME. These methods may perform well for tracers with a high metabolite fraction, in which peak estimation is crucial.

Which Kinetic Model Should be Used?

As described above, IDIF does not usually estimate the peak reliably. This prevents reliable estimation of some of the individual rate constants (K_1, k_2, k_3…), which are highly dependent on the shape of the early part of the curve. We were not surprised to find large and unpredictable errors associated with individual rate constant estimates regardless of the IDIF method used (Zanotti-Fregonara *et al*, 2009*a*, 2011*a*).

When using compartmental modeling, the compound parameters are derived by the individual rate constants. For example, the metabolic rate K_i, which represents the steady-state trapping rate of the tracer in the tissue, is given by K_1k_3/k_2+k_3, the distribution volume V_T is given by K_1/k_2 for one-tissue compartment models and by $K_1/k_2(1+k_3/k_4)$ for two-tissue compartment models. Therefore, errors in estimating rate constants will propagate to some extent to the estimation of compound parameters. It should be noted that these errors originate mainly from a bad estimation of the shape of the input function, rather than a poor identifiability of the constants due, for example, to the noise in the brain or input function time–activity curves. Therefore, the estimation of the compound parameters with a compartment model cannot be improved by a different weighting of the data.

In contrast, graphical approaches (Patlak, Logan) do not require that the shape of the early part of the input function be precisely estimated, as they mainly rely on the area under the curve. Therefore, these methods are more robust with regard to the usual IDIF errors. Using [^{18}F]-FDG and the Patlak plot, Chen *et al* (1998) showed that underestimating the peak by about 20% would cause a $<0.1\%$ variation of the estimated metabolic rates of glucose. Using [^{11}C](*R*)-rolipram and [^{11}C]-PBR28, we found that V_T values calculated with the Logan plot were more accurate than those obtained with compartmental models (Zanotti-Fregonara *et al*, 2011*a*). In addition, graphical approaches are insensitive to peak artifacts due to dispersion and different time-lags of tracer delivery (Guo *et al*, 2007). Graphical methods are nevertheless potentially vulnerable to bias, and this

bias is mostly linked to the accuracy of estimating the later parts of the input functions. Therefore, the most reliable results are obtained by those image-input methods that provide a good estimate of the tail of the curves, which is generally achieved by scaling with blood samples (Zanotti-Fregonara *et al*, 2011*a*). It should be noted, however, that while the estimation of the tail of the whole-blood time–activity curves can be easier than the estimation of the rapidly changing peak, the amount of radiometabolites is generally higher in the tail. Therefore, the results of kinetic modeling using graphical plots are also dependent on the correct estimation of the metabolite-free parent concentration in the tail. As explained above, estimating the metabolite fraction without increasing the invasiveness is a challenging task that only sometimes can be successfully achieved.

Taken together, the results suggest that graphical approaches should be used when compound parameters are the parameters of interest; if individual rate constants are needed, full arterial sampling would be a safer option.

Can Venous Blood Samples be Used Instead of Arterial Blood Samples?

As discussed above, IDIF requires that some blood samples be used to correct for partial volume effects, for radiometabolites, or for both. To avoid arterial cannulation, the only realistic solution would be substituting arterial samples with venous samples. However, as a rule, the arterial tracer kinetics is different from the venous one (Chiou, 1989; Greuter *et al*, 2011). Venous samples can be substituted for arterial samples only when taken during a transient equilibrium phase. Notably, the time when this equilibrium is reached differs for each tracer. For [^{18}F]-FDG, arteriovenous equilibrium is reached about 10 to 15 minutes after injection, and this allows the use of venous samples to calculate IDIF (Chen *et al*, 1998). In contrast, equilibrium is reached only after 20 minutes for α-[^{11}C]-methyl-tryptophan (Nishizawa *et al*, 1998), after 30 to 40 minutes for [^{11}C](*R*)-rolipram (our unpublished data), and never observed over 60 minutes for [^{11}C]-Befloxatone (M Bottlaender, personal communication) and over 3 hours for [^{18}F]-SP203 (our unpublished data). In summary, venous samples can be substituted for arterial samples only for a limited time-window of variable length that must be assessed individually for each tracer. The most straightforward way to overcome this problem would be arterialization of venous blood through heating, which has been successfully employed for different tracers (Backes *et al*, 2009; Moriwaki *et al*, 1993; Phelps *et al*, 1979; Wahl *et al*, 1999; Wong *et al*, 1997). Alternatively, sampling from a different vein may allow investigators to obtain blood concentrations that are closer to those in arterial blood. Ito *et al* (1995) showed that [^{123}I]-IMP radioactivity concentrations were quite different depending on whether they were taken from the cubital vein, the forearm, or a hand vein. Interestingly, hand vein values were consistent with arterial values, and also very similar to concentrations obtained after arterialization of venous blood.

What are the Alternatives?

As discussed above, many shortcomings prevent the widespread use of IDIF in clinical practice. Two methods, alternative to IDIF, are population-based input function (PBIF) and the simultaneous estimation of the input function (SIME). These two methods have the potential, with additional validation and after resolving some methodological issues, to achieve a less-invasive estimation of the input function for some tracers.

Population-based input function uses an appropriately scaled standard input function created by normalizing individual input functions from a population of subjects. For tracers with metabolites, PBIF refers to the serial concentrations over time of the parent radioligand separated from radiometabolites. Population-based input function has been validated mostly for [^{18}F]-FDG, using arterial (Takikawa *et al*, 1993) or venous blood samples (Takagi *et al*, 2004) as scaling factors, or using noninvasive individual parameters such as body surface area (Shiozaki *et al*, 2000) or cerebellar [^{18}F]-FDG activity (Bentourkia, 2006). Studies with other PET tracers are very rare (Beattie *et al*, 2010; Cook *et al*, 1999; Takikawa *et al*, 1994). Nevertheless, PBIF appears to have many practical advantages over IDIF, especially for brain studies where IDIF is more challenging to obtain. Specifically, PBIF does not depend on partial volume effects, scanner characteristics, quality of acquisition, or reconstruction algorithms; it is not operator-dependent; it is generally less time-consuming than IDIF because it does not involve image processing and provides a better estimate of the peak than most IDIF methods. The limitation most commonly attributed to PBIF is that the shape of input function determined in one group (e.g., healthy subjects) may not apply to another group (e.g., patients), because the disease state or its treatment may alter metabolism of the radioligand. We do not think, however, that this is a major problem because, when scaling is performed with blood samples, these samples largely account for the interindividual variability in tracer metabolism and the same PBIF may be applied across different populations of subjects (Zanotti-Fregonara *et al*, 2011*c*). In our opinion, the major limit of this technique is that, just like IDIF, the accuracy of PBIF depends on the metabolite fraction of the tracer. With PBIF, errors in the estimation of the peak are common. As a consequence, when PBIF is applied to [^{11}C](*R*)-rolipram, which has a high parent

concentration at the end of the scan, it gives very reliable results because the peak accounts for a negligible part of the area under the curve (Zanotti-Fregonara *et al*, 2011*c*). However, when applied to [^{11}C]-PBR28, which has a low parent concentration at the end of the scan, the results are much less accurate because the unreliable peak accounts for a larger part of the area under the curve (our unpublished data). Therefore, it is likely that PBIF works better for those same few tracers for which IDIF also works.

The SIME approach seeks to estimate input function parameters simultaneously with kinetic parameters from more than one brain regions and assuming the time–activity curves from these brain regions are different from each other. Recovering the input function common to all regions is accomplished by incorporating the input function parameters into the objective function to be optimized while modeling several ROI data sets simultaneously (Ogden *et al*, 2010). This method has been tested on simulated data (Feng *et al*, 1997; Riabkov and Di Bella, 2002; Wong *et al*, 2002) and in [^{18}F]-FDG studies (Wong *et al*, 2001). Ogden *et al* (2010) recently applied the SIME approach to three neuroreceptor tracers [^{11}C]-DASB, [^{11}C]-BTA, and [^{11}C]-WAY and demonstrated that it can be a valid alternative to full arterial sampling. Although this technique theoretically allows the estimation of a metabolite-corrected input function without blood samples, this requires further validation especially based on the statistical optimization theories and with realistic computer simulations. In practice, at least one blood sample must be collected to ensure identifiability and improve the parameter estimates (Jouvie *et al*, 2011; Ogden *et al*, 2010). Without sampling for the input function, it is not possible to uniquely estimate both the scaling factor for the input function and the parameter K_1, even if the product can be estimated uniquely.

Conclusion

Image-derived input function is an elegant technique for noninvasive estimation of the input function for PET neuroreceptor tracers. However, it is also a challenging technique that can be successfully implemented in clinical practice only for a small number of tracers. Moreover, the use of IDIF rarely translates into a less-invasive procedure for the patients, because arterial blood samples can rarely be avoided. While they still require some blood samples, PBIF and SIME may be valid alternative methods for some tracers.

Acknowledgements

The authors thank Victor W Pike and Sami S Zoghbi for contribution and expertise in radiopharmaceutics. Ioline Henter provided invaluable editorial assistance.

Disclosure/conflict of interest

The authors declare no conflict of interest.

References

Ahn JY, Lee JS, Jang MJ, Lee DS (2000) Noninvasive extraction of input function from carotid artery in H2-15O dynamic brain positron emission tomography using independent component analysis. Second International Workshop on Independent Component Analysis and Blind Signal Separation. Proceedings, pp 493–7

Asselin MC, Cunningham VJ, Amano S, Gunn RN, Nahmias C (2004) Parametrically defined cerebral blood vessels as non-invasive blood input functions for brain PET studies. *Phys Med Biol* 49:1033–54

Backes H, Ullrich R, Neumaier B, Kracht L, Wienhard K, Jacobs AH (2009) Noninvasive quantification of (18)F-FLT human brain PET for the assessment of tumour proliferation in patients with high-grade glioma. *Eur J Nucl Med Mol Imaging* 36:1960–7

Baudrexel A, Graf R, Knoess C, Vollmar S, Wienhard K (2004) Derivation of the input function from dynamic PET images with the HRRT. *IEEE Nucl Sci Symp Conf Rec* 6:3890–2

Beattie BJ, Smith-Jones PM, Jhanwar YS, Schoder H, Schmidtlein CR, Morris MJ, Zanzonico P, Squire O, Meirelles GS, Finn R, Namavari M, Cai S, Scher HI, Larson SM, Humm JL (2010) Pharmacokinetic assessment of the uptake of 16beta-18F-fluoro-5alpha-dihydrotestosterone (FDHT) in prostate tumors as measured by PET. *J Nucl Med* 51:183–92

Beer AJ, Grosu AL, Carlsen J, Kolk A, Sarbia M, Stangier I, Watzlowik P, Wester HJ, Haubner R, Schwaiger M (2007) [F-18]Galacto-RGD positron emission tomography for imaging of alpha v beta 3 expression on the neovasculature in patients with squamous cell carcinoma of the head and neck. *Clin Cancer Res* 13:6610–6

Beierle I, Meibohm B, Derendorf H (1999) Gender differences in pharmacokinetics and pharmacodynamics. *Int J Clin Pharmacol Ther* 37:529–47

Bentourkia M (2005) Kinetic modeling of PET data without blood sampling. *IEEE Trans Nucl Sci* 52:697–702

Bentourkia M (2006) Kinetic modeling of PET-FDG in the brain without blood sampling. *Comput Med Imaging Graph* 30:447–51

Berradja K, Boughanmi N, Bentourkia M (2009) Kinetic modeling of brain FDG data with input function derived from images by independent component analysis. *IEEE Nucl Sci Symp Conf Rec* 2920–3

Bodvarsson B, Mørkebjerg M, Hansen LK, Knudsen GM, Svarer C (2006) Extraction of time activity curves from positron emission tomography: K-means clustering or non-negative matrix factorization (abstract). *Neuroimage* 31(Suppl 1): S154

Brix G, Zaers J, Adam LE, Bellemann ME, Ostertag H, Trojan H, Haberkorn U, Doll J, Oberdorfer F, Lorenz WJ (1997) Performance evaluation of a whole-body PET scanner using the NEMA protocol. *J Nucl Med* 38: 1614–23

Carson R, Planeta-Wilson B, Mulnix T, Frost J (2006) Image based input functions from the carotid arteries with the HRRT. *J Nucl Med* 47 (Suppl 1):57P

Caselli RJ, Chen K, Bandy D, Smilovici O, Boeve BF, Osborne D, Alexander GE, Parish JM, Krahn LE, Reiman

EM (2006) A preliminary fluorodeoxyglucose positron emission tomography study in healthy adults reporting dream-enactment behavior. *Sleep* 29:927–33

Chen K, Bandy D, Reiman E, Huang SC, Lawson M, Feng D, Yun LS, Palant A (1998) Noninvasive quantification of the cerebral metabolic rate for glucose using positron emission tomography, 18F-fluoro-2-deoxyglucose, the Patlak method, and an image-derived input function. *J Cereb Blood Flow Metab* 18:716–23

Chen K, Chen X, Renaut R, Alexander GE, Bandy D, Guo H, Reiman EM (2007) Characterization of the image-derived carotid artery input function using independent component analysis for the quantitation of [18F] fluorodeoxyglucose positron emission tomography images. *Phys Med Biol* 52:7055–71

Chen K, Ge X, Yao L, Bandy D, Alexander GE, Prouty A, Burns C, Zhao X, Wen X, Korn R, Lawson M, Reiman E (2006) An automated normative-based fluorodeoxyglucose positron emission tomography image-analysis procedure to aid Alzheimer disease diagnosis using statistical parametric mapping and interactive image display. *Proc SPIE Int Soc Opt Eng*; Vol. 6144; doi:10.1117/12.651069

Chen KW, Reiman EM, Lawson M, Yun LS, Bandy D, Palant A (1996) Methods for the correction of vascular artifacts in PET 0-15 water brain-mapping studies. *IEEE Trans Nucl Sci* 43:3308–14

Chiou WL (1989) The phenomenon and rationale of marked dependence of drug concentration on blood sampling site. Implications in pharmacokinetics, pharmacodynamics, toxicology and therapeutics (Part II). *Clin Pharmacokinet* 17:275–90

Choi Y, Hawkins RA, Huang SC, Gambhir SS, Brunken RC, Phelps ME, Schelbert HR (1991) Parametric images of myocardial metabolic-rate of glucose generated from dynamic cardiac PET and 2-[F-18]Fluoro-2-Deoxy-D-glucose studies. *J Nucl Med* 32:733–8

Cook GJ, Lodge MA, Marsden PK, Dynes A, Fogelman I (1999) Non-invasive assessment of skeletal kinetics using fluorine-18 fluoride positron emission tomography: evaluation of image and population-derived arterial input functions. *Eur J Nucl Med* 26:1424–9

Croteau E, Lavallee E, Labbe SM, Hubert L, Pifferi F, Rousseau JA, Cunnane SC, Carpentier AC, Lecomte R, Benard F (2010) Image-derived input function in dynamic human PET/CT: methodology and validation with (11)C-acetate and (18)F-fluorothioheptadecanoic acid in muscle and (18)F-fluorodeoxyglucose in brain. *Eur J Nucl Med Mol Imaging* 37:1539–50

Everett BA, Oquendo MA, Abi-Dargham A, Nobler MS, Devanand DP, Lisanby SH, Mann JJ, Parsey RV (2009) Safety of radial arterial catheterization in PET research subjects. *J Nucl Med* 50:1742

Fadaili el M, Zanotti-Fregonara P, Souloumiac A, Tavitian B, Ribeiro MJ, Trebossen R (2009) Extraction of arterial input function from dynamic PET brain images using nonnegative sources separation. *ESMI P* 075

Feng D, Wong KP, Wu C, Siu W (1997) A technique for extracting physiological parameters and the required input function simultaneously from PET image measurements: theory and simulation study. *IEEE Trans Inform Tech Biomed* 1:243–54

Fueger BJ, Czernin J, Cloughesy T, Silverman DH, Geist CL, Walter MA, Schiepers C, Nghiemphu P, Lai A, Phelps ME, Chen W (2010) Correlation of 6-18F-fluoro-L-dopa PET uptake with proliferation and tumor grade in newly diagnosed and recurrent gliomas. *J Nucl Med* 51:1532–8

Fung EK, Planeta-Wilson B, Mulnix T, Carson R (2009) A multimodal approach to image-derived input functions for brain PET. *IEEE Nucl Sci Symp Conf Rec (1997)*, pp 2710–4

Gambhir SS, Schwaiger M, Huang SC, Krivokapich J, Schelbert HR, Nienaber CA, Phelps ME (1989) Simple noninvasive quantification method for measuring myocardial glucose utilization in humans employing positron emission tomography and fluorine-18 deoxyglucose. *J Nucl Med* 30:359–66

Greuter H, Lubberink M, Hendrikse NH, Van der Veldt AA, Wong Y, Schuit R, Windhorst AD, Boellaard R, Lammertsma AA (2011) Venous versus arterial blood samples for plasma input pharmacokinetic analysis of different radiotracer PET studies. *J Nucl Med* 52(Suppl 1):1974

Guo H, Renaut RA, Chen K (2007) An input function estimation method for FDG-PET human brain studies. *Nucl Med Biol* 34:483–92

Henriksen G, Spilker ME, Sprenger T, Hauser AI, Platzer S, Boecker H, Toelle TR, Schwaiger M, Wester HJ (2006) Gender dependent rate of metabolism of the opioid receptor-PET ligand [18F]fluoroethyldiprenorphine. *Nuklearmedizin* 45:197–200

Ichise M, Liow JS, Lu JQ, Takano A, Model K, Toyama H, Suhara T, Suzuki K, Innis RB, Carson RE (2003) Linearized reference tissue parametric imaging methods: application to [^{11}C]DASB positron emission tomography studies of the serotonin transporter in human brain. *J Cereb Blood Flow Metab* 23:1096–112

Ishiwata K, Itou T, Ohyama M, Yamada T, Mishina M, Ishii K, Nariai T, Sasaki T, Oda K, Toyama H, Senda M (1998) Metabolite analysis of [11C]flumazenil in human plasma: assessment as the standardized value for quantitative PET studies. *Ann Nucl Med* 12:55–9

Ito H, Koyama M, Goto R, Kawashima R, Ono S, Atsumi H, Ishii K, Fukuda H (1995) Cerebral blood flow measurement with iodine-123-IMP SPECT, calibrated standard input function and venous blood sampling. *J Nucl Med* 36:2339–42

Jouvie C, de Gavriloff S, Santiago-Ribeiro MJ, Gaura V, Remy P, Zanotti-Fregonara P, Maroy R (2011) Simultaneous estimation of input functions: the B-SIME method. Biomedical imaging: From Nano to Macro, *2011 IEEE International Symposium on; 2011*, 1758–61

Kim KM, Watabe H, Shidahara M, Ahn JY, Choi S, Kudomi N, Hayashida K, Miyake Y, Iida H (2001) Noninvasive estimation of cerebral blood flow using image-derived carotid input function in H215O dynamic PET. *Nuclear Science Symposium Conference Record, 2001 IEEE*; 3:1282–5

Kimura Y, Ishii K, Fukumitsu N, Oda K, Sasaki T, Kawamura K, Ishiwata K (2004) Quantitative analysis of adenosine A1 receptors in human brain using positron emission tomography and [1-methyl-11C]8-dicyclopropylmethyl-1-methyl-3-propylxanthine. *Nucl Med Biol* 31:975–81

Kreisl WC, Fujita M, Fujimura Y, Kimura N, Jenko KJ, Kannan P, Hong J, Morse CL, Zoghbi SS, Gladding RL, Jacobson S, Oh U, Pike VW, Innis RB (2010) Comparison of [(11)C]-(R)-PK 11195 and [(11)C]PBR28, two radioligands for translocator protein (18 kDa) in human and monkey: implications for positron emission tomographic imaging of this inflammation biomarker. *Neuroimage* 49:2924–32

Krejza J, Arkuszewski M, Kasner SE, Weigele J, Ustymowicz A, Hurst RW, Cucchiara BL, Messe SR (2006)

Carotid artery diameter in men and women and the relation to body and neck size. *Stroke* 37:1103–5
Lammertsma AA, Bench CJ, Hume SP, Osman S, Gunn K, Brooks DJ, Frackowiak RS (1996) Comparison of methods for analysis of clinical [11C]raclopride studies. *J Cereb Blood Flow Metab* 16:42–52
Liptrot M, Adams KH, Martiny L, Pinborg LH, Lonsdale MN, Olsen NV, Holm S, Svarer C, Knudsen GM (2004) Cluster analysis in kinetic modelling of the brain: a noninvasive alternative to arterial sampling. *Neuroimage* 21:483–93
Litton JE (1997) Input function in PET brain studies using MR-defined arteries. *J Comput Assist Tomogr* 21: 907–9
Lopresti BJ, Klunk WE, Mathis CA, Hoge JA, Ziolko SK, Lu X, Meltzer CC, Schimmel K, Tsopelas ND, DeKosky ST, Price JC (2005) Simplified quantification of Pittsburgh Compound B amyloid imaging PET studies: a comparative analysis. *J Nucl Med* 46:1959–72
Ludemann L, Sreenivasa G, Michel R, Rosner C, Plotkin M, Felix R, Wust P, Amthauer H (2006) Corrections of arterial input function for dynamic (H2OPET)-O-15 to assess perfusion of pelvic tumours: arterial blood sampling versus image extraction. *Phys Med Biol* 51: 2883–900
Maroy R, Jouvie C, De Gavriloff S, Gaura V, Remy P, Santiago-Ribeiro MJ, Trebossen R (2011) Fully automated and minimally invasive estimation of the input function and of the regional glucose consumption in [18F]-FDG PET exams of the human brain. *J Nucl Med* 52(Suppl 1): 158
Mitkovski S, Villemagne VL, Novakovic KE, O'Keefe G, Tochon-Danguy H, Mulligan RS, Dickinson KL, Saunder T, Gregoire MC, Bottlaender M, Dolle F, Rowe CC (2005) Simplified quantification of nicotinic receptors with 2[18F]F-A-85380 PET. *Nucl Med Biol* 32:585–91
Moriwaki H, Matsumoto M, Hashikawa K, Oku N, Okazaki Y, Handa N, Kimura K, Kozuka T, Kamada T, Nishimura T (1993) [Quantitative assessment of cerebral blood flow by 123I-IMP SPECT: venous sampling method with hand warming in the water bath]. *Kaku Igaku* 30:481–8
Mourik JE, Lubberink M, Klumpers UM, Comans EF, Lammertsma AA, Boellaard R (2008*a*) Partial volume corrected image derived input functions for dynamic PET brain studies: methodology and validation for [11C]flumazenil. *Neuroimage* 39:1041–50
Mourik JE, Lubberink M, Schuitemaker A, Tolboom N, van Berckel BN, Lammertsma AA, Boellaard R (2009) Image-derived input functions for PET brain studies. *Eur J Nucl Med Mol Imaging* 36:463–71
Mourik JE, van Velden FH, Lubberink M, Kloet RW, van Berckel BN, Lammertsma AA, Boellaard R (2008*b*) Image derived input functions for dynamic high resolution research tomograph PET brain studies. *Neuroimage* 43:676–86
Naganawa M, Kimura Y, Ishii K, Oda K, Ishiwata K, Matani A (2005*a*) Extraction of a plasma time-activity curve from dynamic brain PET images based on independent component analysis. *IEEE Trans Biomed Eng* 52:201–10
Naganawa M, Kimura Y, Nariai T, Ishii K, Oda K, Manabe Y, Chihara K, Ishiwata K (2005*b*) Omission of serial arterial blood sampling in neuroreceptor imaging with independent component analysis. *Neuroimage* 26: 885–90
Nishizawa S, Leyton M, Okazawa H, Benkelfat C, Mzengeza S, Diksic M (1998) Validation of a less-invasive method for measurement of serotonin synthesis rate with alpha-[11C]methyl-tryptophan. *J Cereb Blood Flow Metab* 18:1121–9
Ogden RT, Zanderigo F, Choy S, Mann JJ, Parsey RV (2010) Simultaneous estimation of input functions: an empirical study. *J Cereb Blood Flow Metab* 30:816–26
Parker BJ, Feng DG (2005) Graph-based Mumford-Shah segmentation of dynamic PET with application to input function estimation. *IEEE Trans Nucl Sci* 52:79–89
Phelps ME, Huang SC, Hoffman EJ, Selin C, Sokoloff L, Kuhl DE (1979) Tomographic measurement of local cerebral glucose metabolic rate in humans with (F-18)2-fluoro-2-deoxy-D-glucose: validation of method. *Ann Neurol* 6:371–88
Reiman EM, Chen KW, Alexander GE, Caselli RJ, Bandy D, Osborne D, Saunders AM, Hardy J (2004) Functional brain abnormalities in young adults at genetic risk for late-onset Alzheimer's dementia. *Proc Natl Acad Sci USA* 101:284–9
Riabkov DY, Di Bella EVR (2002) Estimation of kinetic parameters without input functions: analysis of three methods for multichannel blind identification. *IEEE Trans Biomed Eng* 49:1318–27
Sanabria-Bohorquez SM, Labar D, Leveque P, Bol A, De Volder AG, Michel C, Veraart C (2000) [11C]flumazenil metabolite measurement in plasma is not necessary for accurate brain benzodiazepine receptor quantification. *Eur J Nucl Med* 27:1674–83
Sanabria-Bohorquez SM, Maes A, Dupont P, Bormans G, de Groot T, Coimbra A, Eng W, Laethem T, De Lepeleire I, Gambale J, Vega JM, Burns HD (2003) Image-derived input function for [11C]flumazenil kinetic analysis in human brain. *Mol Imaging Biol* 5:72–8
Sayre G, Seo Y (2009) Extracting purely image-derived arterial input functions from the carotid artery using a generalized expectation-maximization algorithm with partial volume correction for PET-CT studies of head and neck cancer. *Proc World Mol Imaging Congress P* 1144
Schiepers C, Chen W, Cloughesy T, Dahlbom M, Huang SC (2007*a*) 18F-FDOPA kinetics in brain tumors. *J Nucl Med* 48:1651–61
Schiepers C, Chen W, Dahlbom M, Cloughesy T, Hoh CK, Huang SC (2007*b*) 18F-fluorothymidine kinetics of malignant brain tumors. *Eur J Nucl Med Mol Imaging* 34:1003–11
Schiepers C, Czernin J, Hoh CK, Nuyts J, Phelps ME, Dahlbom M (2002*a*) Factor analysis for automatic determination of myocardial flow in N-13-ammonia PET studies. *J Nucl Med* 43:52
Schiepers C, Hoh CK, Dahlbom M, Wu HM, Phelps ME (1998) Reproducibility of input functions obtained with factor analysis in breast cancer. *J Nucl Med* 39:165
Schiepers C, Hoh CK, Nuyts J, Seltzer M, Wu C, Huang SC, Dahlbom M (2008) 1-C-11-acetate kinetics of prostate cancer. *J Nucl Med* 49:206–15
Schiepers C, Hoh CK, Nuyts J, Wu HM, Phelps ME, Dahlbom M (2002*b*) Factor analysis in prostate cancer: delineation of organ structures and automatic generation of in- and output functions. *IEEE Trans Nucl Sci* 49:2338–43
Schiepers C, Hoh CK, Seltzer MA, Phelps ME, Dahlbom M (2000) Factor analysis for quantification of acetate PET in primary prostate cancer. *J Nucl Med* 41:100
Schiepers C, Wu HM, Nuyts J, Dahlbom M, Hoh CK, Huang SC, Phelps ME (1997) F-18 fluoride PET: is non-invasive quantitation feasible with factor analysis? *J Nucl Med* 38:343

Shields AF, Briston DA, Chandupatla S, Douglas KA, Lawhorn-Crews J, Collins JM, Mangner TJ, Heilbrun LK, Muzik O (2005) A simplified analysis of [18F]3′-deoxy-3′-fluorothymidine metabolism and retention. *Eur J Nucl Med Mol Imaging* 32:1269–75

Shiozaki T, Sadato N, Senda M, Ishii K, Tsuchida T, Yonekura Y, Fukuda H, Konishi J (2000) Noninvasive estimation of FDG input function for quantification of cerebral metabolic rate of glucose: optimization and multicenter evaluation. *J Nucl Med* 41:1612–8

Su KH, Wu LC, Liu RS, Wang SJ, Chen JC (2005) Quantification method in [18F]fluorodeoxyglucose brain positron emission tomography using independent component analysis. *Nucl Med Commun* 26: 995–1004

Takagi S, Takahashi W, Shinohara Y, Yasuda S, Ide M, Shohtsu A, Seio T (2004) Quantitative PET cerebral glucose metabolism estimates using a single non-arterialized venous-blood sample. *Ann Nucl Med* 18:297–302

Takikawa S, Dhawan V, Chaly T, Robeson W, Dahl R, Zanzi I, Mandel F, Spetsieris P, Eidelberg D (1994) Input functions for 6-[fluorine-18]fluorodopa quantitation in parkinsonism: comparative studies and clinical correlations. *J Nucl Med* 35:955–63

Takikawa S, Dhawan V, Spetsieris P, Robeson W, Chaly T, Dahl R, Margouleff D, Eidelberg D (1993) Noninvasive quantitative fluorodeoxyglucose PET studies with an estimated input function derived from a population-based arterial blood curve. *Radiology* 188:131–6

Trebossen R, Bendriem B, Ribeiro MJ, Sarazin M, Strul D, Dupont F, Semah F, Remy P (1999) Quantifying cerebral PET with FDG using dynamic internal carotid arteries imaging. *IEEE Nucl Sci Symp Conf Rec* 3:1737–40

van der Weerdt AP, Klein LJ, Boellaard R, Visser CA, Visser FC, Lammertsma AA (2001) Image-derived input functions for determination of MRGlu in cardiac F-18-FDG PET scans. *J Nucl Med* 42:1622–9

Verhaeghe J, Gravel P, Mio R, Fukasawa R, Rosa-Neto P, Soucy JP, Thompson CJ, Reader AJ (2010) Motion compensation for fully 4D PET reconstruction using PET superset data. *Phys Med Biol* 55:4063–82

Visvikis D, Francis D, Mulligan R, Costa DC, Croasdale I, Luthra SK, Taylor I, Ell PJ (2004) Comparison of methodologies for the *in vivo* assessment of 18FLT utilisation in colorectal cancer. *Eur J Nucl Med Mol Imaging* 31:169–78

Wahl LM, Asselin MC, Nahmias C (1999) Regions of interest in the venous sinuses as input functions for quantitative PET. *J Nucl Med* 40:1666–75

Wang WL, Georgi JC, Nehmeh SA, Narayanan M, Paulus T, Bal M, O'Donoghue J, Zanzonico PB, Schmidtlein CR, Lee NY, Humm JL (2009) Evaluation of a compartmental model for estimating tumor hypoxia via FMISO dynamic PET imaging. *Phys Med Biol* 54:3083–99

Wang WL, Lee NY, Georgi JC, Narayanan M, Guillem J, Schoder H, Humm JL (2010) Pharmacokinetic analysis of hypoxia F-18-fluoromisonidazole dynamic PET in head and neck cancer. *J Nucl Med* 51:37–45

Wienhard K (2002) Measurement of glucose consumption using [F-18]fluorodeoxyglucose. *Methods* 27: 218–25

Wong DF, Young D, Wilson PD, Meltzer CC, Gjedde A (1997) Quantification of neuroreceptors in the living human brain: III. D2-like dopamine receptors: theory, validation, and changes during normal aging. *J Cereb Blood Flow Metab* 17:316–30

Wong KP, Feng DG, Meikle SR, Fulham MJ (2001) Simultaneous estimation of physiological parameters and the input function *in vivo* PET data. *IEEE Trans Inf Technol B* 5:67–76

Wong KP, Meikle SR, Feng D, Fulham MJ (2002) Estimation of input function and kinetic parameters using simulated annealing: application in a flow model. *IEEE Trans Nucl Sci* 49:707–13

Wu HM, Hoh CK, Choi Y, Schelbert HR, Hawkins RA, Phelps ME, Huang SC (1995) Factor-analysis for extraction of blood time-activity curves in dynamic FDG-PET studies. *J Nucl Med* 36:1714–22

Zanotti-Fregonara P, Fadaili el M, Maroy R, Comtat C, Souloumiac A, Jan S, Ribeiro MJ, Gaura V, Bar-Hen A, Trebossen R (2009*a*) Comparison of eight methods for the estimation of the image-derived input function in dynamic [(18)F]-FDG PET human brain studies. *J Cereb Blood Flow Metab* 29:1825–35

Zanotti-Fregonara P, Liow JS, Fujita M, Dusch E, Zoghbi SS, Luong E, Boellaard R, Pike VW, Comtat C, Innis RB (2011*a*) Image-derived input function for human brain using high resolution PET imaging with [C](R)-rolipram and [C]PBR28. *PloS One* 6:e17056

Zanotti-Fregonara P, Maroy R, Comtat C, Jan S, Gaura V, Bar-Hen A, Ribeiro MJ, Trebossen R (2009*b*) Comparison of 3 methods of automated internal carotid segmentation in human brain PET studies: application to the estimation of arterial input function. *J Nucl Med* 50:461–7

Zanotti-Fregonara P, Maroy R, Sureau F, Comtat C, Jan S, Syrota A, Trebossen R (2007) Noninvasive quantification of the cerebral metabolic rate of 18F-FDG in dynamic brain PET studies using an image-derived input function. *Eur J Nucl Med Mol I* 34:S144

Zanotti-Fregonara P, Zoghbi SS, Liow JS, Luong E, Boellaard R, Gladding RL, Pike VW, Innis RB, Fujita M (2011*b*) Kinetic analysis in human brain of [11C](R)-rolipram, a positron emission tomographic radioligand to image phosphodiesterase 4: a retest study and use of an image-derived input function. *Neuroimage* 54: 1903–9

Zanotti-Fregonara P, Zoghbi SS, Liow JS, Luong E, Boellaard R, Gladding RL, Pike VW, Innis RB, Fujita M (2011*c*) Population-based input function is an accurate alternative to arterial sampling in [11C](R)-rolipram PET brain studies. *J Nucl Med* 52(Suppl 1): 548